Master of Science dissertation:

Evaluation of methods for MR imaging near metallic hip prostheses

Fredrik Wellman

Supervisor:

Sven Månsson

This work has been performed at the Department of Medical Radiation Physics, Skåne University Hospital, Malmö

Department of Medical Radiation Physics, Clinical Sciences, Lund
Lund University, Sweden, 2011

Abstract

Introduction

Failure of metallic hip prosthesis is a growing problem, and has triggered the interest for MRI-diagnosis, which is a superior technique when imaging soft-tissue. View-angle-tilting (VAT) and Slice Encoding for Metal Artifact Correction (SEMAC) are MR-techniques for suppression of in-plane and through-plane distortions, respectively. A combination of the VAT and SEMAC techniques allows visualization of tissues near, or directly at, the surface of metal prostheses, and can therefore reveal pathology not accessible by CT or X-ray, since MRI is better at imaging soft-tissue.

Aim

The aim of this master thesis was to develop techniques for quantitative evaluation of the artifacts that arise when metal prostheses are imaged with MRI, and to compare MRI pulse sequences with different techniques for artifact suppression. Three hip prostheses, made of different materials, were imaged and the artifacts were quantified with respect to both slice bending (through-plane) and in-plane artifact size.

Materials and methods

Three hip prostheses (Birmingham Hip Resurfaring (BHR) consisting mainly of Cobalt-Chromium (Co-Cr), Stryker Exeter primarily made of stainless steel and Stryker Omnifit with a titanium shaft and steel head) were embedded into agarose gel together with a rectilinear Perspex grid. The true extents of the prostheses were determined by an x-ray projection. A coronal MR image of each prosthesis, where the image-plane coincides with the grid-plane, was acquired on a 1.5-T scanner (Siemens Avanto, equipped with new pulse sequences for implant imaging (WARP package)). Three types of MRI pulse sequences were evaluated: Optimized TSE: a standard turbo spin echo with optimized acquisition parameters for imaging near metallic objects, VAT: a turbo spin echo with view-angle tilting, SEMAC: a turbo spin echo with both VAT and slice distortion correction (6, 10 and 16 z-phase encoding (PE) steps used). All sequences had a voxel size of 0.74 x 0.74 x 3 mm^3. The slice bending artifacts (through-plane distortions) were quantified by adding together the length of the visible gridlines of the central slice and dividing by the true length. The in-plane artifacts were quantified by dividing the artifact area with the true prosthesis area but also by using a mask. For quantification of total artifacts a binary distortion-free mask was created from the x-ray projection and the best SEMAC sequence image. The mask was subtracted from the images resulting in an artifact-image, consisting of the pile-up and loss of signal. The quantification was made using the sum of squares of the artifact-images.

Discussion

The VAT sequence reduces in-plane artifacts compared to an optimized TSE sequence, but does not address artifacts from a distorted slice profile. The SEMAC sequence significantly reduces both types of artifacts, at the price of a much prolonged scan time. The titanium prosthesis produced much smaller artifacts than the Co-Cr prostheses and could be almost perfectly reproduced using the SEMAC sequence. The results indicate that SEMAC with more phase-encoding steps achieves a more artifact-free image since it corrects for both in-plane and through-plane distortions. The accuracy of the mask method was compromised by the mask pixel size being not much smaller than the grid thickness. This may be improved by higher image resolution or using a non-binary mask.

Conclusion

Through-plane distortions were successfully quantified by measuring the length of the visible gridlines. Quantification of in-plane distortions by regions of interest also produced results in agreement with the visual impressions of the artifacts, however with the drawback of being operator dependent and subjective. The mask based methods have potential for quantifying the combined effects of in-plane and through-plane distortions without user input, but require further improvements. The VAT-sequence reduced much of the in-plane distortions, but no through-plane distortions. The SEMAC-sequence reduced both in-plane and through-plane distortions, however in this study, at least 16 z-phase encoding steps were needed, which requires a very long scan time. The results demonstrate that the effects of pulse sequence type, parameter settings, and prosthesis material can be quantitatively evaluated by the proposed grid-based phantom and analysis methods.

Utvärdering av olika MR-tekniker som kan se nära höftproteser av metall

Magnetresonanstomografi (MR) är en metod för att ta skiktbilder inuti kroppen. Denna metod utnyttjar det faktum att en väldigt stor magnet kommer att påverka vätekärnorna i våra kroppar. Genom att skicka in radiovågor i kroppen kan en spole samla upp den information som studsar tillbaka och med denna information kan man skapa skiktbilder inuti kroppen. Alla metoder som gör att man kan ”se in i kroppen” har ett stort värde inom sjukvården.

Det har blivit mer och mer vanligt med medicinska problem när man opererar in höftproteser hos människor. Detta har ökat intresset för att använda MR-bildtagning, som är en utmärkt metod att använda för att studera mjukvävnad, vid diagnosticering utav dessa besvär. Eftersom höftproteserna oftast består av metall kommer detta att innebära ett problem och det blir ett fel i bilden (så kallade ”artefakter” uppstår) nära metallobjekten, vilket gör att läkare inte kan ge en säker diagnos på vad som orsakar besvär nära protesen. View-angle-tilting (VAT) och Slice Encoding for Metal Artifact Correction (SEMAC) är olika metoder inom MR som används för att minska problemet utav metallobjektens närhet hos MR-bilder. En kombination utav både VAT och SEMAC möjliggör att man kan titta på vävnad både nära och i direkt anslutning till metallproteser och kan därför avslöja sjuk vävnad som inte kan ses utav skiktröntgen och röntgen.

Målet med detta examensarbete var att utveckla olika metoder för att utvärdera de artefakter som uppkommer när MR-bilder tas på olika metallproteser samt att jämföra de olika MR-teknikerna för bildtagning avsedd att reducera dessa typer av artefakter. MR-bilder togs på tre olika så kallade fantomer, som är tre olika höftproteser tillverkade utav olika material inbakade i agerosgel tillsammans med ett rutnät. Artefakterna bestämdes med de två allvarligaste felen i åtanke: där ett är att man får skeva bilder (distortioner) i själva bildplanet, dvs. det skiktet av volymen som kommer ge en bild och det andra är att man får böjda snitt, det vill säga att den skiktbild som fås inte är plan utan är böjd.

Snittböjningsartefakterna (felaktiga genom bildplanet) bestämdes genom att summera längden av de synliga rutnätslinjerna hos det centrala snittet och dividera dem med den sanna längden. Artefakterna i bildplanet bestämdes genom att dividera artefaktarean med den sanna protesarean men också genom att använda en mask. För att bestämma de totala artefakterna skapades en binär distortionsfri mask från röntgenprojektioner och den bästa SEMAC-sekvensbilden. Masken subtraherades från bilderna vilket resulterade i en artefaktbild, som består av signaluppbyggnader och signalförluster. Själva mätvärdet som erhölls fick man fram genom att ta kvadratsumman av artefaktbilderna.

VAT-metoden reducerar artefakter i bildplanet jämfört med den optimerade vanliga metoden som används på sjukhuset idag. SEMAC-sekvensen reducerar båda typer av artefakter, men kräver mycket lång tid för att få fram bilder. Protesen som är gjord av titan ger upphov till mycket mindre artefakter jämfört med de andra proteserna, som är gjorda utav kobolt-krom och rostfritt stål.

Artefakterna genom bildplanet blev framgångsrikt bestämda genom att mäta längden av det synliga rutnätet. Bestämningen av artefakterna i bildplanet genom att dividera areaorna gav resultat som stämmer väl överens med det visuella intryck man får utav artefakterna. Denna mätning har dock nackdelen att de är beroende av vem som gör den. De maskbaserade metoderna har en potential för att bestämma alla artefakter utan att använda sig utav användarinmatning, men kräver ytterligare förbättringar. Dessa resultat demonstrerar att effekterna av MR-metod för bildtagning och protesmaterialet kan utvärderas med de föreslagna rutnätsbaserade fantomen och de föreslagna analysmetoderna.

Contents

Abbrevations and acronyms

FOV – Field of View
GRAPPA – GeneRalized Autocalibrating Partially Parallel Acquisitions
IP – In-plane
iPAT – integrated Parallel Acquisition Technique
MRI – Magnetic Resonance Imaging
PACS – Picture Archiving and Communication System
PE – z-phase-encoding
SEMAC – Slice Encoding for Metal Artifact Correction
TP – Through-plane
TSE – Turbo Spin Echo
VAT – View Angle Tilting
WIP – Work In Progress

1 Introduction

1.1 Background

Metallic implants are very common in orthopedic surgery and are used, for example, with joint replacement (arthroplasty) to ease chronic joint conditions and arthritic joints, to align vertebra in case of severe scoliosis and may also be used to fixate fractures. In the United States the amount of primary total hip arthroplasties performed were substantially increased between 1990 and 2002 [1] and the number is expected to accelerate throughout the next several decades [2]. Installation of prostheses may cause several different complications, for example, prosthesis-loosening, infections, fractures and also metallosis, where metallic debris from the prostheses is built-up in the soft-tissue near the prosthesis and ultimately causing necrosis [3, 4]. The standard modality to diagnose these complications is by using conventional x-ray. Conventional x-ray however requires the x-ray beams to be exactly parallel to the bone-implant interface and any obliquity can obscure the radiolucent area, thus conventional x-ray often fails to diagnose pathological conditions, which are later identified using invasive methods [5]. Another modality is Computed Tomography (CT). CT can identify patterns of bone loss and osteolytisc lesion [6], however it exposes patient to a significant amount of ionizing radiation and does not have the soft-tissue contrast to identify early stages of complications. Also it suffers heavily from beam-hardening artifacts and loss of data through the field of view [7]. Magnetic Resonance Imaging (MRI) has, with its supreme soft-tissue contrast, a great potential to be the best modality to diagnose these complications. MRI, however, suffers heavily from metal-induced artifacts, which stems from the magnetic field inhomogeneities caused by metallic implants [8].

There are several different methods which can suppress these metal-induced artifacts, including single point imaging [9], Pre-Polarized MRI [10, 11], Reversed Polarity Gradient Acquisitions [12, 13], Short Echo-Time Projection Reconstruction[14, 15], View-Angle Tilting (VAT) [16], Slice Encoding for Metal Artifact Correction (SEMAC) [17] and Multi-Acquisition Variable-Resonance Image Combination (MAVRIC) [18]. A work-in-progress (WIP) pulse-sequence package (from collaboration between the Radiology Department at SUS Malmö and Siemens), which utilizes the VAT and SEMAC imaging techniques, has been evaluated in this work and compared to standard turbo spin echo (TSE) sequences.

1.2 Aims and purpose

This work aims at quantifying the artifacts that arise when metal prostheses are imaged with different MRI-techniques that reduce metal-induced artifacts. For the radiologist, it is important to know how well these techniques correct metal-induced artifacts and what kind of new artifacts that might be introduced, in order to select an optimal examination protocol.

The purpose of this study was therefore to develop methods for quantitative evaluation of metal artifacts and to compare different MRI techniques for metal-artifact reduction (VAT and SEMAC), to see which of these methods that would be most suitable in clinical applications.

2 Theory

2.1 Metal artifacts

Metallic implants will cause distortion of both the static (B_0) and the dynamic (B_1) magnetic fields of the MR scanner. Distortions to the B_1 field alter the signal intensity, while B_0 affects both signal intensity and mechanisms of the spatial encoding. For conventional pulse sequences, such as spin echo and gradient echo, B_0-artifacts dominate over B_1-artifacts at 1.5T and 3.0T. Because of this, only the effects of the B_0-artifacts are explained in this work. Artifacts will also result from eddy currents on the metal surface and radiofrequency shielding effects, which however are not discussed further in this work.

2.1.1 Magnetic susceptibility

The B_0 field of an MRI magnet with empty bore is typically homogeneous within a couple of ppm (1 ppm ~60Hz at 1.5T) over the central volume in the magnet. When a patient is put into the MRI-system there is an increase in heterogeneity in the order of hundreds of hertz, which in turn is compensated with electromagnetic shim gradients. A metallic object increases the heterogeneity with tens of kHz (around 100 ppm). This kind of heterogeneity cannot be compensated with shimming. The magnetic susceptibility (χ) is the material property which determines the increased heterogeneity. For tissue and bone, the magnetic susceptibility is around -10 ppm, which can be compared to the magnetic susceptibility for metals such as titanium, cobalt-chromium and stainless steel, which are 182 ppm, 900 ppm and 3000-5000 ppm respectively.

2.1.2 T_2^* dephasing

T_2^* can be described as the local through-voxel B_0 gradients acting as an effective transverse relaxation mechanism. Near metallic objects the so called T_2^*-dephasing is extremely fast because of the steep field gradients near the metallic object. Gradient-echo images will have large signal voids near the metallic implants because of the T_2^*-dephasing, however by using a simple spin-echo sequence, this effect is minimized.

2.1.3 Frequency encoding artifacts

The reconstruction requires the frequency-encoding gradient (G_{freq}) to be linear as a function of the spatial coordinate x. This linearity is compromised near a metallic object, resulting in a faulty positioning of the signal. Spin with a position x which is resonating at a metal-induced off-resonance frequency of δf will be mis-encoded to a position:

$$x' = x + \frac{\delta f}{G_{freq}} \tag{2.1.1}$$

G_{freq} (unit: Hz/m) in itself is related to the receiver bandwidth (BW_{freq}) and field of view (FOV_x) through:

$$G_{freq} = \frac{BW_{freq}}{FOV_x} \tag{2.1.2}$$

Combining equations 2.1.2 and 2.1.1 result in:

$$x' = x + FOV_x \cdot \frac{\delta f}{BW_{freq}} \tag{2.1.3}$$

So according to equation 2.1.3 above the displacements increase with increasing FOV and is reduced with higher receiving bandwidth. The distortions affecting the frequency-encoding are in this work referred to as in-plane (IP) distortions.

Also worth mentioning is that the phase-encoding is not compromised by the metallic object, since the off-resonance effects all phase-encoding steps equally.

2.1.4 Slice selection

The slice selection is the process of applying a gradient (G_{slice}) while simultaneously exposing the imaged object to a RF-field with an off-resonance frequency δf_{RF} and bandwidth BW_{Slice} which in turn results in an excitation of a slab with thickness:

$$\delta z = \frac{BW_{Slice}}{G_{slice}} \tag{2.1.4}$$

at a position given by:

$$z_0 = \frac{\delta f_{RF}}{G_{slice}} \tag{2.1.5}$$

When a metallic object is nearby this process is compromised in a similar manner as the frequency encoding. Since the G_{slice} gradient will no longer be linear, a rectangular slab will no longer be linear, both the slice thickness and the slice position will be affected, resulting in a curved slice. The distortions affecting the slice-encoding are in this work referred to as through-plane (TP) distortions.

2.1.5 General remedy for reduction of metal-induced artifacts

Learning from the theory above, the general remedy for reduction of metal-induced artifacts is to use a 2D spin-echo based pulse sequence with a high receiver bandwidth. The slices should also be as thin as possible and a high excitation bandwidth for the RF-pulses is preferred to maximize the slice-selection gradient, which can be achieved by using a short RF-pulse, or a sinc RF-pulse with many lobes.

2.2 View Angle Tilting (VAT)

View Angle Tilting, or VAT, was first introduced in a paper by Cho *et. al* [16], where it was intended for correction of both chemical shifts and susceptibility-induced B_0-inhomogeneity. The main idea is to apply the slice selection gradient during the readout, which has the effect of tilting the view angle with $\theta = tan^{-1}\left(G_{slice}/G_{freq}\right)$ where G_{slice} and G_{freq} is the slice selective gradient and readout gradient respectively. In a conventional SE-acquisition, during the slice selection, all flipped spin are precessing at a frequency within a narrow band (i.e. the slice selection bandwidth). When the gradient is removed, the spins no longer experience the same magnetic field because of the inhomogeneities, which means that they no longer have

the same Larmor frequency. In order for them to have the same Larmor frequency, during the frequency encoding, the same gradient used for the slice selection can be applied at the same time as the readout gradient [19].

In an article by Butts *et. al* [20], it is said that the correction requires the same magnitude and direction as the slice selective gradient and that this method relies on the fact that off-resonance result in a displacement in both the slice-selective and readout gradient. When this is viewed from an angle, these two displacements work together in order to get off-resonance-signals to appear registered. A schematic view of how this can be seen in figure 2.2.1 below.

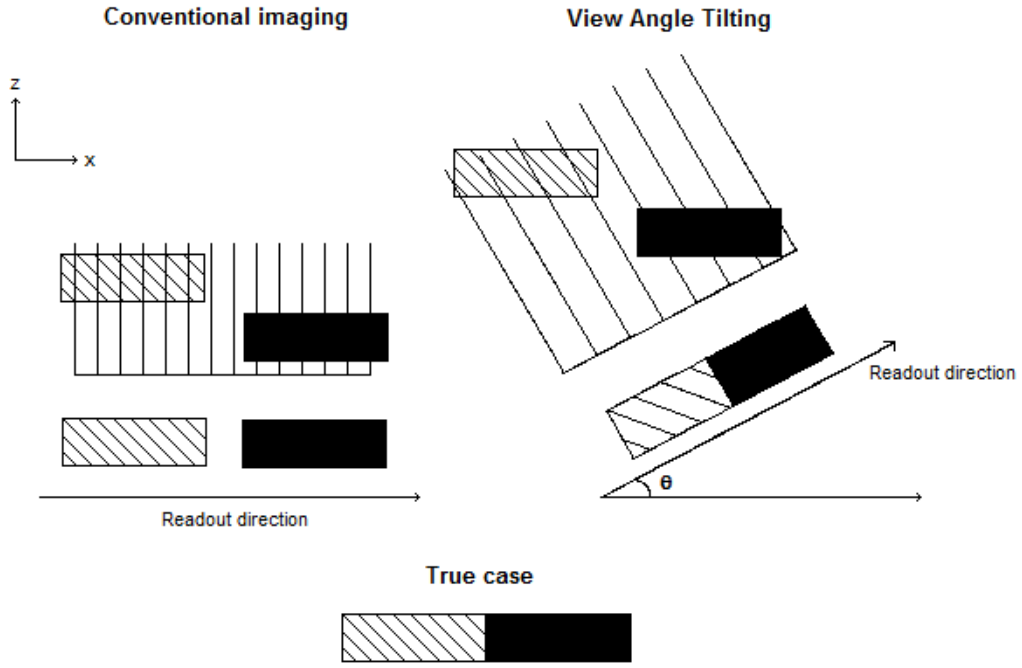

Figure 2.2.1 Schematic view of the process of view angle tilting. It can be seen that by tilting the view angle, a distortion otherwise showing two close items as separate instead, with VAT, shows them together, as is the true case. Off-resonance spin results in shifts in both slice and readout direction as is described in previous sections. These off-resonant spins are then re-registered when the slice selection gradient is applied, though which a projection through the slice at the tilted view angle. Figure from reference [20].

It shall be noted that VAT does not come complication free, since while tilting the view angle, the image becomes blurred. This has been investigated by Butts *et. al* [21] determining that the slice profile modulation, causing an effective low-pass filter of the data is the source of the blurring.

2.3 Slice Encoding for Metal Artifact Correction (SEMAC)

The main theory of Slice Encoding for Metal Artifact Correction, or SEMAC, stems from the original article, written by Wenmiao Lu *et al.* [17] in 2009. More information is also drawn from the article "Accelerated Slice Encoding for Metal Artifact Correction" written by Brian A. Hargreaves *et al.* in 2010 [22].

Images acquired near or through metal prostheses suffer from spatially dependent artifacts, i.e. signal pile-ups and signal voids, which is a result of the non-linear frequency-position mapping, also described in section 2.1 above. This affects frequency-encoding (causing in-plane (IP) distortions) and slice selection (causing through-plane (TP) distortions).

SEMAC is a pulse sequence which corrects both in-plane and through-plane distortions. The sequence is a Spin-Echo pulse sequence using a VAT compensation gradient and adding extra phase-encoding (PE) steps in the slice direction (along the z-axis). The schematics of the pulse sequence can be seen in figure 2.3.1 below.

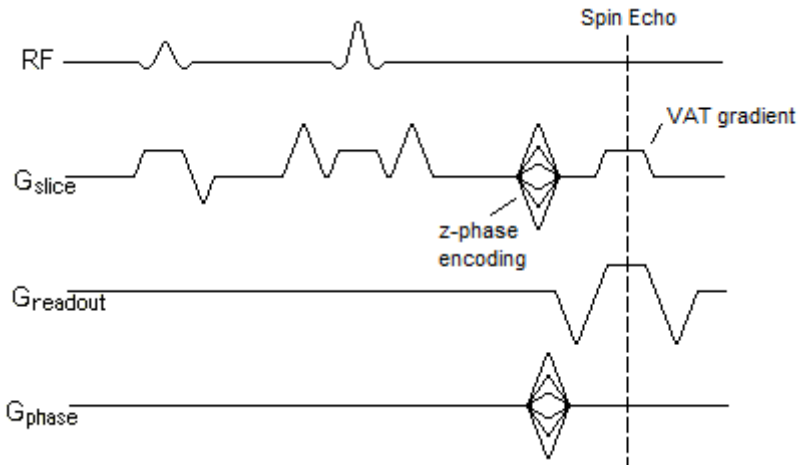

Figure 2.3.1 shows the SEMAC sequence where the extra z-phase encoding and the applied VAT gradient can be seen. Figure adapted from [17].

2.3.1 The distorted slice profile

If m(x,z) is the spin density at position (x,z), and Δf(x,z) is the field inhomogeneity at position (x,z) (the actual position is (x,y,z), however since the phase encoding direction (y-direction) do not have any distortion this notation is dropped to simplify the equations), the resulting excited magnetization with a distorted excitation profile, m_e, can be expressed as:

$$m_e(x,z) = m(x,z) \cdot \prod\left[\frac{\frac{\gamma}{2\pi}G_{slice}z + \Delta f(x,z) - f_e}{B_{RF}}\right] = m(x,z) \cdot \prod\left[\frac{z - \Delta z(x,z) - z_0}{s}\right] \quad (2.3.1)$$

where B_{RF} is the bandwidth of the RF-pulse, G_{slice} is the slice selection gradient, $\gamma/2\pi$ is the gyromagnetic ratio (42,58 MHz/T for the proton), z_0 is the nominal slice location excited at a

transmit frequency $f_e = \frac{\gamma}{2\pi} G_{slice} z_0$ and Δz is the through-plane shift for a spin with field inhomogeneity Δf, which is:

$$\Delta z = -\frac{\Delta f}{\frac{\gamma}{2\pi} G_{slice}} = -\frac{\Delta f}{B_{RF}} s \tag{2.3.2}$$

where s is the nominal slice thickness, given by $s = \frac{2\pi B_{RF}}{\gamma G_{slice}}$. $\prod(f/B_{RF})$ is the frequency profile of the RF pulse, ideally a rectangular function defined by:

$$\prod(f/B_{RF}) = \begin{cases} 1, \text{ if } |f| \leq B_{RF}/2 \\ 0, \text{ otherwise} \end{cases}$$

$m_e(x,z)$ will contain spins from different slice locations, for which $|z - \Delta z(x,z) - z_0| \leq s/2$ because of the field inhomogeneities caused by the metal object. Because of this Δz(x,z) describes the distorted excitation profile caused by Δf(x,z).

2.3.2 The SEMAC sequence

If N_z is the number of z-phase encoding steps with an amplitude gradient of G_{zi} and with a duration of T_z, the resolution of the z-phase encoding is determined by $\delta_s = 2\pi/(\gamma N_z G_{zi} T_z)$. The VAT compensation gradient, applied during the readout, is G_{slice}. According to Lu *et. al.* [17], at time t and the n:th z-phase encoding step, the received signal is:

$$r(t,n) = \int_z \left(\int_x m_e(x,z) exp\big[-i\big(\gamma G_{freq} x + \gamma G_{slice} z + 2\pi \Delta f(x,z)\big)t\big] dx \right) exp[-in\gamma G_{zi} T_z z] dz \tag{2.3.3}$$

Looking closer at the VAT-compensation gradient during the readout:

$$\begin{aligned} &\int_x m_e(x,z) exp\left[-i\left(\gamma G_{freq} x + \gamma G_{slice} z + 2\pi \Delta f(x,z)\right)t\right] dx \\ &= \int_x m_e(x,z) exp\big[-i\big(\gamma G_{freq} x + \gamma G_{slice}(z - \Delta z(x,z) - z_0) + 2\pi f_e\big)t\big] dx \\ &= \int_x m_e(x,z) exp\left[-i\left(\gamma G_{freq}\left(x + \frac{G_{slice}}{G_{freq}} \delta z(x,z)\right) + 2\pi f_e\right)t\right] dx \end{aligned} \tag{2.3.4}$$

where $\delta z = z - \Delta z(x,z) - z_0$ is the uncertainty of determining the slice locations of the spins in the distorted slice, where $\delta z \leq s/2$, this equation show that δz is responsible for in-plane distortions left uncorrected $\delta x = \frac{G_{slice}}{G_{freq}} \delta z$, because of the encoded x-location is given by:

$$x' = x + \frac{G_{slice}}{G_{freq}} \delta z(x,z) = x + \delta x(x,z) \tag{2.3.5}$$

In terms of pixels, the uncorrected in-plane distortion is bounded by:

$$\delta z_{max} = \frac{B_{RF}/2}{B_p} \tag{2.3.6}$$

where $B_p = 2B_{read}/N_x$ is the readout bandwidth per pixel (with B_{read} the readout bandwidth and N_x the number of readout samples).

It can be seen from equation 2.3.4 that the VAT gradient also modulates the excited spin at a transmit frequency, f_e, At the case of several excited slices, every slice must be demodulated with its transmit frequency so that the slices do not have relative in-plane shifts. The demodulated signal r(t,u) at f_e is described by:

$$\begin{aligned} r(t,u) &= \int_z \left(\int_x m_e(x,z) exp\left[-i\gamma G_{freq}(x + \delta x(x,z))t\right] dx \right) exp[-ink_{zi}z] dz \\ &= \int_z \left(\int_x m_e(x,z) exp\left[-i\gamma G_{freq} x' t\right] dx \right) exp[-ink_{zi}z] dz \end{aligned} \tag{2.3.7}$$

where $k_{zi} = \gamma G_{zi} T_z$ is the stepping of the z-phase encoding. Also note that the z-phase encoding will have a field of view (FOV_z) given by $2\pi/k_{zi}$ and must be sufficiently large to avoid aliasing in the resolved excitation profile (see figure 2.3.3 below).

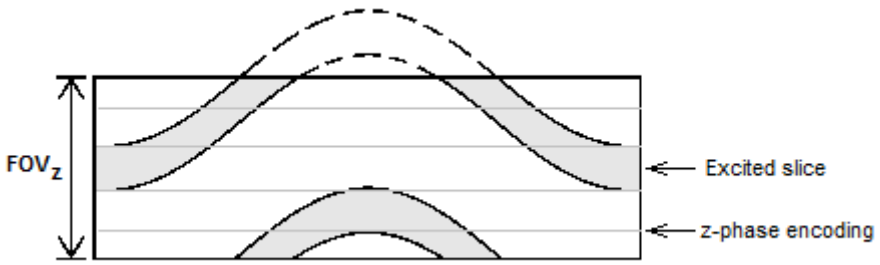

Figure 2.3.2.1 shows the aliasing effect stemming from insufficient amounts of PE steps.

2.3.3 Through-plane distortion correction

According to Lu *et. al.* [17], the spatial distribution of the magnetization $m_e(x,z)$ is fully resolved with a invers Fourier transform of the signal r(t,u) from equation 2.3.7. Multiple slices are required for correction of through-plane distortions since pile-ups in one slice corresponds to a signal loss in other slices. Metal-induced field inhomogeneities cause complicated distorted excitation profiles, curved slices as mentioned above. In order to cover all spins in a region-of-interest (ROI), a sufficient number of slices, N_s, are chosen. The excitation profile of each slice is then resolved with the z-phase-encoding (PE), so that during the image reconstructed each spin in the ROI is positioned back to their actual voxel location. Each spin in every voxel is then summed, which corrects the through-plane distortions. Note that by just doing a direct summation results in a serious signal loss because the spin resolved from the different slices may have relative phases. The sum of the magnitude removes the relative phase between the slices; however, the magnitude operation causes the background noise to become Rayleigh-distributed, so that the noise no longer has a mean of zero [23]. By summing non-zero mean, this degrades the resulting SNR. The relative phases are taken care of by carefully adjust the RF-phase reference and/or the receive phase reference [24]. Since all slices thereby have equal phase, each resolved spin can be summed without using the magnitude operation.

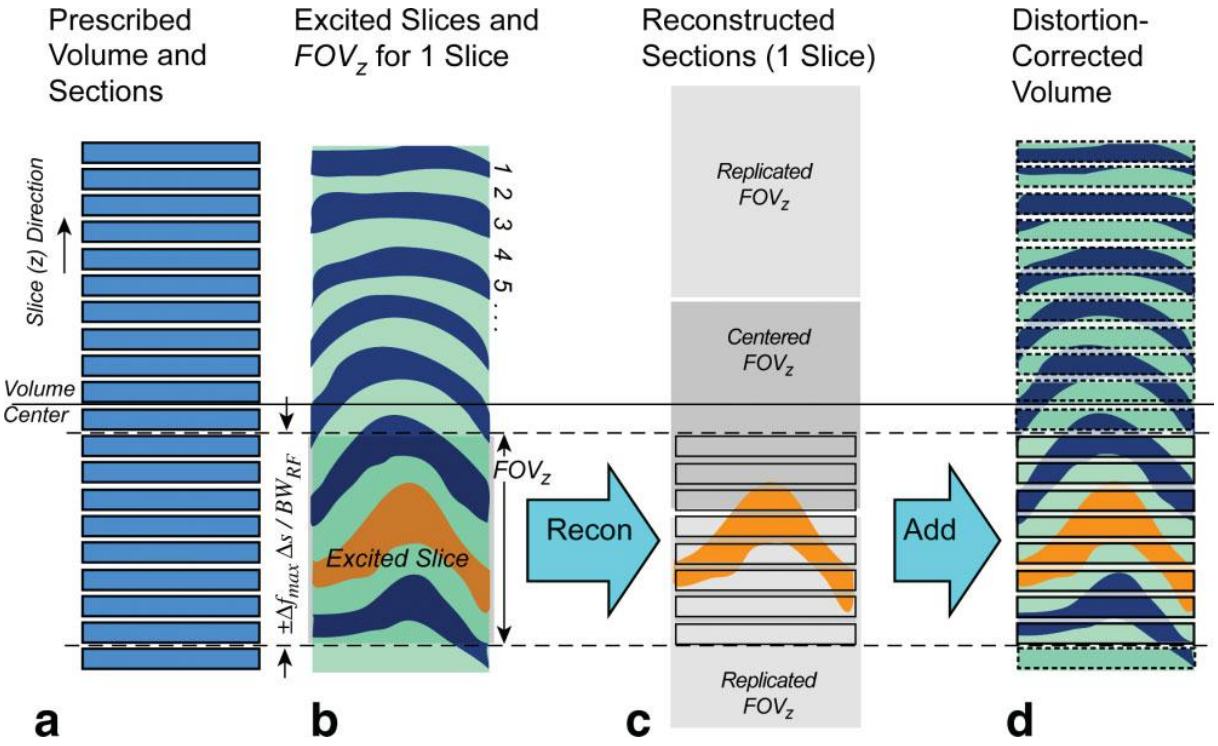

Figure 2.3.3.1 schematically shows how the SEMAC sequence works. The prescribed slices (**a**) differ from the actually excited slices (**b**) since the field inhomogeneities caused by the metal prosthesis alter both the shape and the thickness of the slices. Each slice is encoded into a 3D-volume by the z-phase-encoding gradient, where the FOV_z must be large enough to cover the expected slice distortion (**c**). A distortion corrected volume is obtained by adding together the 3D-volumes from all excited slices (**d**). Figure from reference [22].

3 Materials and methods

3.1 Phantoms

Three phantoms were used in this study, consisting of containers with three different hip prostheses embedded in agarose gel together with a rectilinear Perspex grid. The three prostheses used in the phantoms were a Birmingham Hip Resurfacing (BHR) prosthess, a Stryker Exeter total hip replacement prosthesis and a Stryker Omnifit total hip replacement prosthesis. The agarose gel was used mainly to provide a mechanical fixation of the prostheses, but also to provide a signalgenerating medium with tissue-like relaxation times. A mixture containing 44.5 gram agar, 1.25 grams of Nickel(II) nitrate Hexahydrate and 2500 ml of water were used to create the gel. The gel was made by mixing the agarose and nickel salt together and then letting the mixture reach boiling temperature. Later the mixture was left cooling to around 40 degrees Celsius. The prosthesis was suspended to the container using normal sewing thread. The gel was then poured into the container, covering a little less than half of the prosthesis carefully to avoid air bubbles. Remaining air bubbles were then removed. The gel was left to harden in a refrigerator over the night. Later more gel was created using the process described above. The rectilinear Perspex grid (dimensions 135x195 mm and 3 mm thick) was cut to fit the prosthesis and put into the container so that the grid covered the middle of the prosthesis (Fig 3.1.2). More gel was poured over to cover the remaining parts of the prosthesis. Figures 3.1.1-3 below show the different steps in the process of the phantom making.

Figure 3.1.1 The Omnifit prosthesis in the container before pouring in the gel.

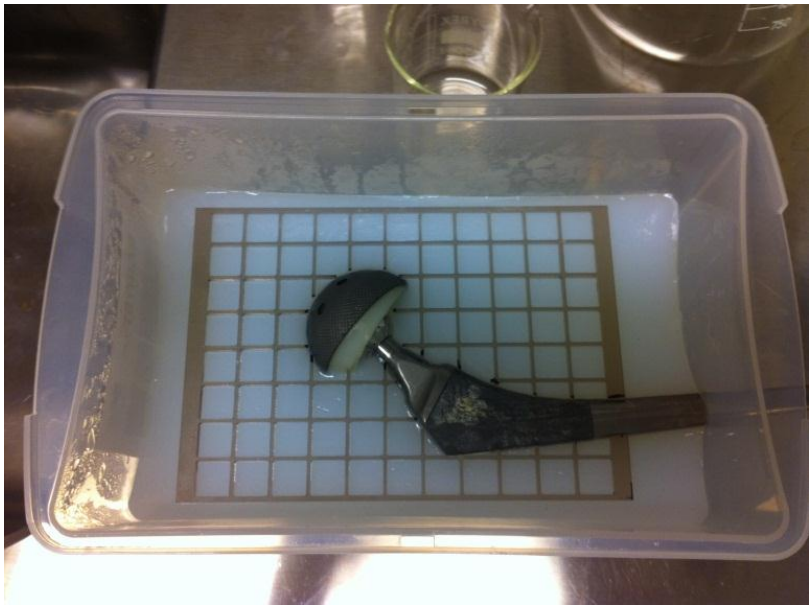

Figure 3.1.2 The Omnifit prosthesis with half the container filled with agarose gel and the rectilinear grid put in place.

Figure 3.1.2 The Omnifit prosthesis phantom complete with the top layer of agarose gel still waiting to harden.

3.2 MR-imaging

Five images were primarily used in this master thesis, one using a turbo-spin echo (TSE) with parameters optimized for imaging near metallic objects, the WARP sequence with only VAT and three different images using SEMAC with three different amounts of PE steps: 6, 10 and 16 PE steps. MR images of the phantoms described above were acquired using a Siemens Avanto 1.5 T system. Table 3.2.1 below shows all the parameters used for the different pulse sequences. These parameters remained the same for all the different phantoms.

Table 3.2.1 shows all the different parameters used for each pulse sequence.

Parameter	**TSE**	**VAT**	**SEMAC 6 PE**	**SEMAC 10 PE**	**SEMAC 16 PE**
# of slices	17	17	17	17	17
Slice thickness [mm]	3	3	3	3	3
Echo Time (TE) [ms]	5	5.6	5.6	5.6	5.6
Repetition Time (TR) [ms]	480	500	480	480	820
Readout bandwidth (BW_{read}) [Hz/Px]	751	971	977	977	977
FOV_{read} [mm]	380	380	380	380	380
FOV_{phase} [mm]	380	380	380	380	380
Number of excitations (NEX)	3	3	1	1	1
SEMAC Phase encoding steps	-	Off	6	10	16
iPAT (GRAPPA acceleration factor)	-	-	2	2	3

3.3 Image matching using Adobe Photoshop™

The knowledge of the true extent of the prostheses in the phantoms is needed for the artifact measurement described in section 3.5, but was also made to visually see the true prostheses extent when viewing the MR images. For this, x-ray images were taken and then matched to the MR images. This match was made manually by using Adobe Photoshop 6.0. The x-ray images were taken with brass bars taped on the sides of the containers. This gave the knowledge of knowing were edges of the container where in the x-ray image and this was the method in which the match was made. In figure 3.3.1 a matched MR image can be seen for the Omnifit phantom with the standardized turbo spin echo (TSE) protocol.

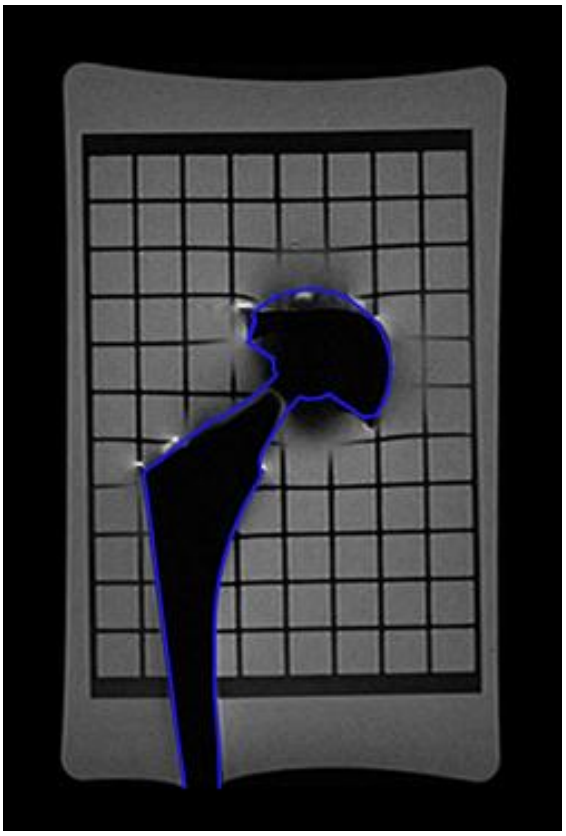

Figure 3.3.1 Standardized TSE protocol for the Omnifit phantom. The blue line represents the true extent of the prosthesis.

3.4 Through-plane distortion quantification

Through-plane distortion bends the slices, making the grid become less visible with greater through-plane distortion. Since the visible grid length reflects the presence of through-plane distortions this measurement was developed as a means to try to quantify the through-plane distortion.

For this method the MR images in the middle of the prosthesis were used. The visible grid length was then measured by using different tools in the Picture Archiving and Communication System (PACS) of Skåne University Hospital. The quantification was made by taking the sum of measured length and dividing them by the sum of the true grid length,

which was measured from the grid before it was put into the phantom (Corrected for the grid length cut away to fit the prostheses). The quantifier Q_d is thus determined by:

$$Q_d = \frac{\sum Visible\ grid\ length}{\sum True\ grid\ length} \tag{3.4.1}$$

This measurement was made such that a distortion-free image would have a value of 100%. An example of how this measurement was made can be seen in figure 3.4.1 below.

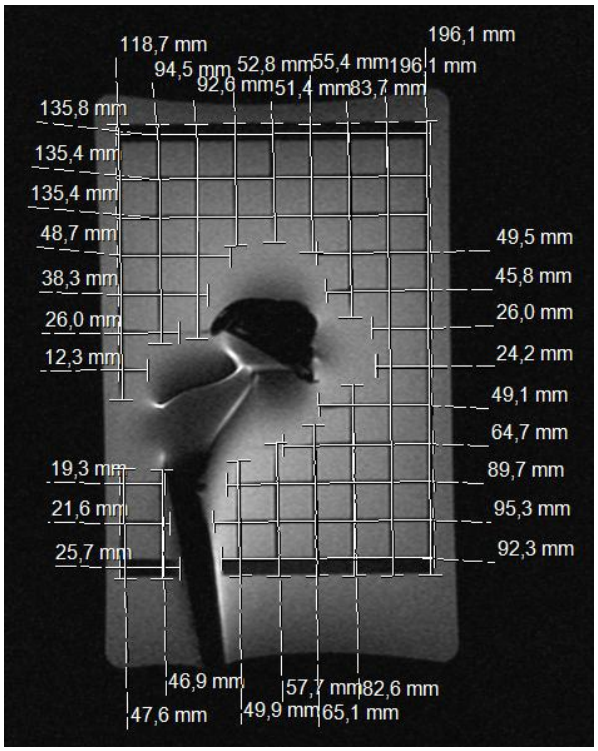

Figure 3.4.1 Example-image of the through-plane distortion quantification made in PACS for the Exeter Total Hip Replacement phantom. This image illustrates how the visible grid length was measured.

3.5 Area measurements

Another measurement made to try to quantify the artifacts was the area measurement. This measurement was a way to try to compare the extent of the artifacts in the image with a distortion-free case, i.e. the true extent of the prostheses determined by x-ray projections. This was made using Adobe Photoshop 6.0 and a program called ImageJ, which is an image processing and analysis tool. Regarding the window settings, the image was scaled between the lowest and highest pixel value, with the center in the middle between these values, so all the intensities could be seen in the images. Using Photoshop, the extent of the artifacts was first approximated by roughly drawing an area, which covers the prosthesis and artifact area (see image 3.5.1 below). This area was then compared to the area of the true extent of the prosthesis, also determined using Photoshop. Using ImageJ, the pixels of the areas could be counted. The quantification was made dividing the artifact area with the area from the true extent of the prosthesis. The quantifier Q_a, is determined by:

$$Q_a = \frac{N_2 - N_1}{N_2} \quad (3.5.1)$$

Where Q is the quantifier, N_1 is the number of pixels in the area drawn in the MR-image and N_2 is the number of pixels in the area comprising the "true extent" of the prosthesis, i.e. the pixels in the area of the x-ray prosthesis.

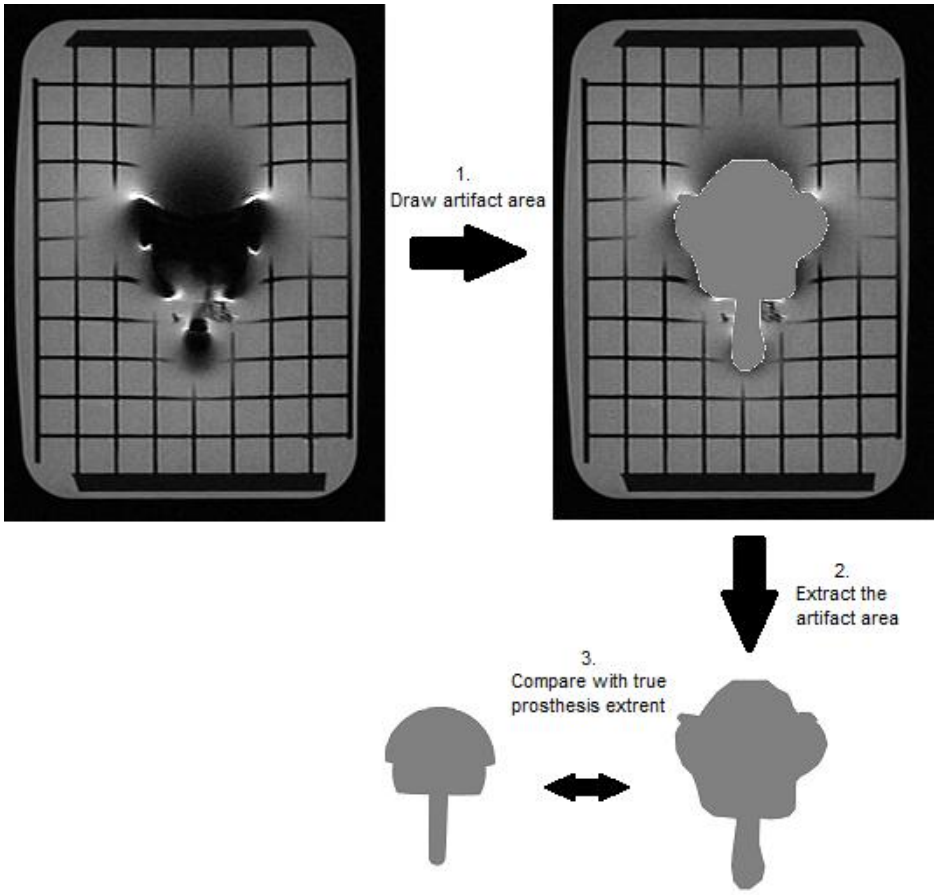

Figure 3.5.1 Schematic figure showing how the area measurement was made. First an artifact area was approximated and drawn from the MR-images, then that area was extracted using Adobe Photoshop and lastly compared to the true extent of the prosthesis.

3.6 Mask measurements

The problems with the earlier methods are that they contain a high amount of subjectivity. Since the lines are drawn from hand in the through-plane distortion quantification, it differs from person to person where these lines end. Since we do not have an abrupt transition from where the grid starts to where the gel is in the MR-images we do not know where to stop the lines being drawn. Since the area is arbitrarily drawn to try to fit in the area where the artifacts start, the area measurement is also highly subjective. The mask measurement was created to lessen the degree of subjectivity, doing this by creating a binary, so called, mask, which resembles a perfect MR-image, free from distortion artifacts.

The mask measurement starts out by creating a binary image from the respective MR-images. First the extents of the prostheses were determined with help from the x-ray images. This was done using Adobe Photoshop. Using the best SEMAC sequence images the grid was approximately drawn in Photoshop. The extents of the prostheses and the grids where then put together in a preliminary template. This template was later read into Matlab and from there the binary image was created, resulting in a value of 1 where the gel is and 0 otherwise. In order to complete the mask, which at first only contains information of the prostheses and the grid, the shape of the container had to be accounted for as well, by placing zeros in the background outside of the container. This was done in Matlab using the respective MR-images that are to be compared to the mask. A schematically figure describing the process of creating the mask is shown in figure 3.6.1 below. Because of this each image thus has a corresponding mask. These masks were then compared with the different images using the three methods described in sections 3.6.1, 3.6.2 and 3.6.3. The resulting image was evaluated by calculating a quantifier of total artifact ("image quality" value V) according to:

$$V = \sum_{x,y} \left(I_{image}(x,y) - I_{mask}(x,y) \right)^2 \qquad (3.6.1)$$

where x and y are the image coordinates and I_{image} and I_{mask} are the pixel values of the MR-images and the mask respectively. This equation assumes that the value I_{image} is 1 in the gel and 0 in the grid.

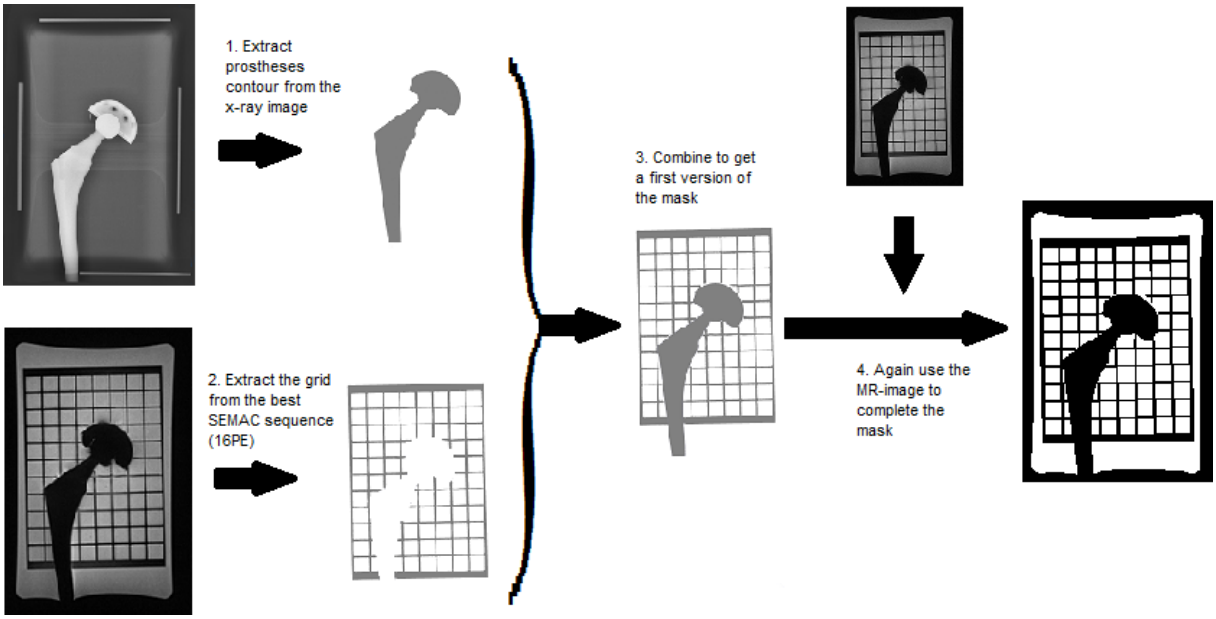

Figure 3.6.1 schematically shows the process of creating the binary mask. First the contour of the prostheses were determined using x-ray, then the grid was drawn and determined using the best SEMAC sequence (16 PE steps). By combining the grid and the prosthesis contour ends up in a first version of the mask, which is then completed by using the respective MR-images to draw out the shape of the container, ending up in a specific mask for each MR-image to be compared to the mask.

3.6.1 Binary method

With the binary mask created, the main problem was how to use it in order to compare it with the MR-images and thus getting quantitative data. The first method tested was the binary method. With this method the original MR-image was altered and made into a binary image, so that it would be easily comparable to the mask by using equation 3.6.1 above. First for each set, i.e. all the images for a certain type of prosthesis, all MR-images where scaled such that their mean intensity were equal to the mean of the SEMAC (PE 16) image. This was done in order for the different MR-images to be comparable to one another. In order to create a binary MR-image, a threshold had to be chosen, i.e. a value were pixels above would gain the value 1 and equal to or below, will have a value of 0. This is because we have the signal from the gel in the mask representing the value 1. Several different thresholds were tested, however the most suitable would be one that would be in the middle between the largest (a region in the gel) and the lowest (a region in the grid) pixel value, which was found to roughly correspond to three times the value of the mean for each set of MR-images. Figure 3.6.1 shows the binary image created from the optimized protocol MR-image for the Stryker Exeter prosthesis.

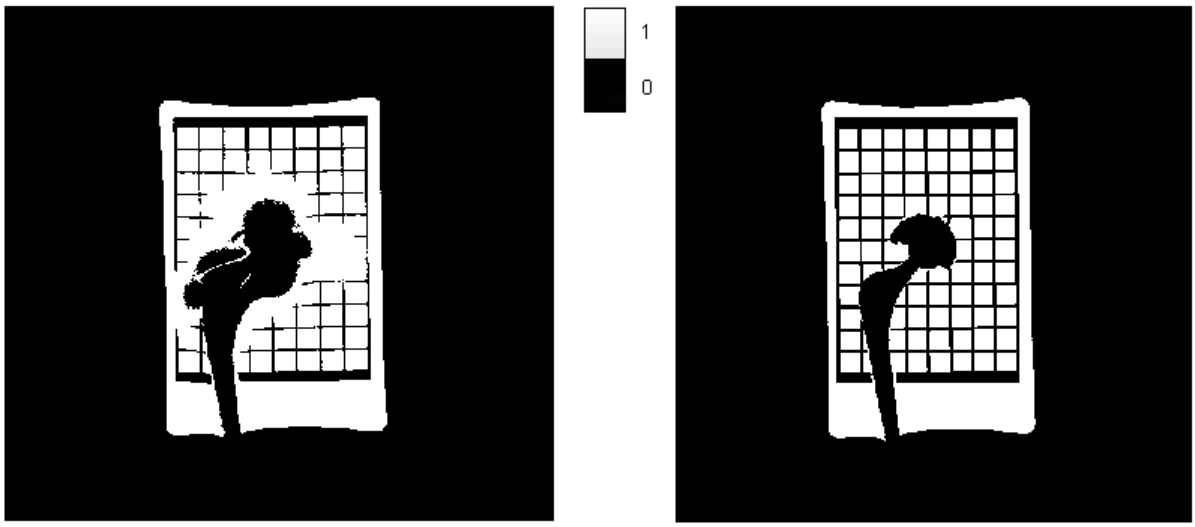

Figure 3.6.1.1 Left: The binary image created from the standardized optimized protocol MR-image for the Exeter prosthesis. The values of the x- and the y-axis show the respective pixel position and the scale to the right shows that we have the value 1 for the gel-signal and 0 otherwise. *Right:* The corresponding binary mask.

3.6.2 Non-binary method: Uncorrected Gel normalization

The problem with the binary method described above is the alteration of the original MR-images into binary image. Another approach is instead to use the real MR-images for the quantification. Modifications of the original MR-images are still needed for this approach, however not as exaggerated as making the MR-images binary. The hope with this method is to receive even better quantification because the binary method is more subjective; it requires the usage of subjectively and arbitrarily chosen threshold values to make the MR-images binary.

This method is based on the idea of adjusting the signal in the MR-images such that the pixel values in the gel are 1 and the pixel values in the grid are 0, making it comparable to the binary mask, which also has a signal value of 1 in the gel and 0 in the grid. This was done by first removing any traces of signal from corresponding darker area in the MR-images, since the mask has pixel values of 0 outside the gel location (and in the grid). This was done by subtracting all pixel values in the MR images with the mean value of a region in the MR-images that are expected to have a value of 0, in this case the uppermost thick part of the grid. Any values lower than zero was set to zero. Then the signal needed to be normalized and the value used to do this adjustment is the pixel values of the image is the mean value in a chosen region of interest at the position in the gel presumed to be as homogeneous as possible, i.e. a region were no signal variations are supposed to exist as a consequence of the metallic object. By doing the procedure described above and subtracting the MR-image with the mask, the result is an image consisting of only the residual artifacts. The artifact image itself shows, in an ideal case, only signal caused by artifacts. The purpose itself is to detect these artifacts, which is seen as both signal pile-ups and the signal losses. The quantitative data from these artifact-images are simply the sum of squares of the artifact image.

3.6.3 Non-binary method: Corrected Gel normalization

In the non-binary method described above the gel signal value in a region not affected by metal-induced artifact is presumed to be 1. However, this ideal case is not true; in fact the gel signal was inhomogeneous, varying rougly in the range of 0.6-1.4 for the Omnifit phantom, 0.9-1.3 for the BHR phantom and 0.6-1.2 for the Exeter phantom. This signal variation stems mainly from local coil insensitivities, which can be corrected for.

This correction, which tries to balance out the intensity in the image, was implemented by fitting a two-dimensional, second order polynomial surface to the gel pixels in the MR-image and then dividing the image by the polynomial surface, pixel-by-pixel. This correction was only used for the non-binary mask method and no for the methods described in section 3.4 and 3.5.

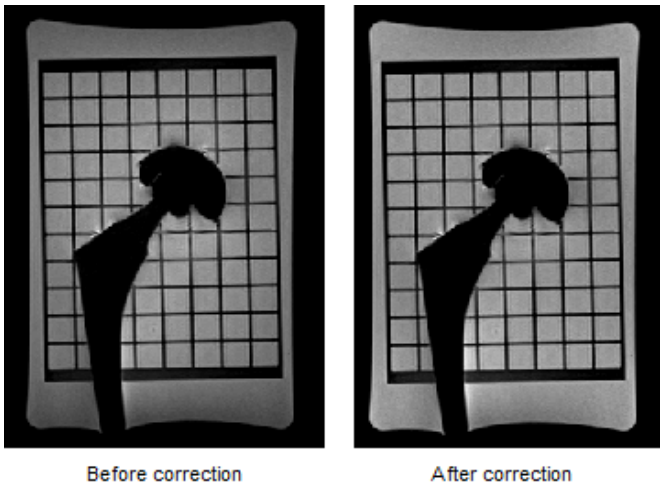

Figure 3.6.3.1 The MR images of the Omnifit phantom using the SEMAC sequence with 16 PE steps showed before (left) and after (right) the intensity normalization.

4 Results

4.1 MR-images

Figure 4.1 displays the MR-images taken with the different pulse sequences. The x-ray contours of the prostheses are marked red for the Birmingham Hip Resurfacing (BHR) prosthesis, blue for the Omnifit prosthesis and green for the Exeter prosthesis.

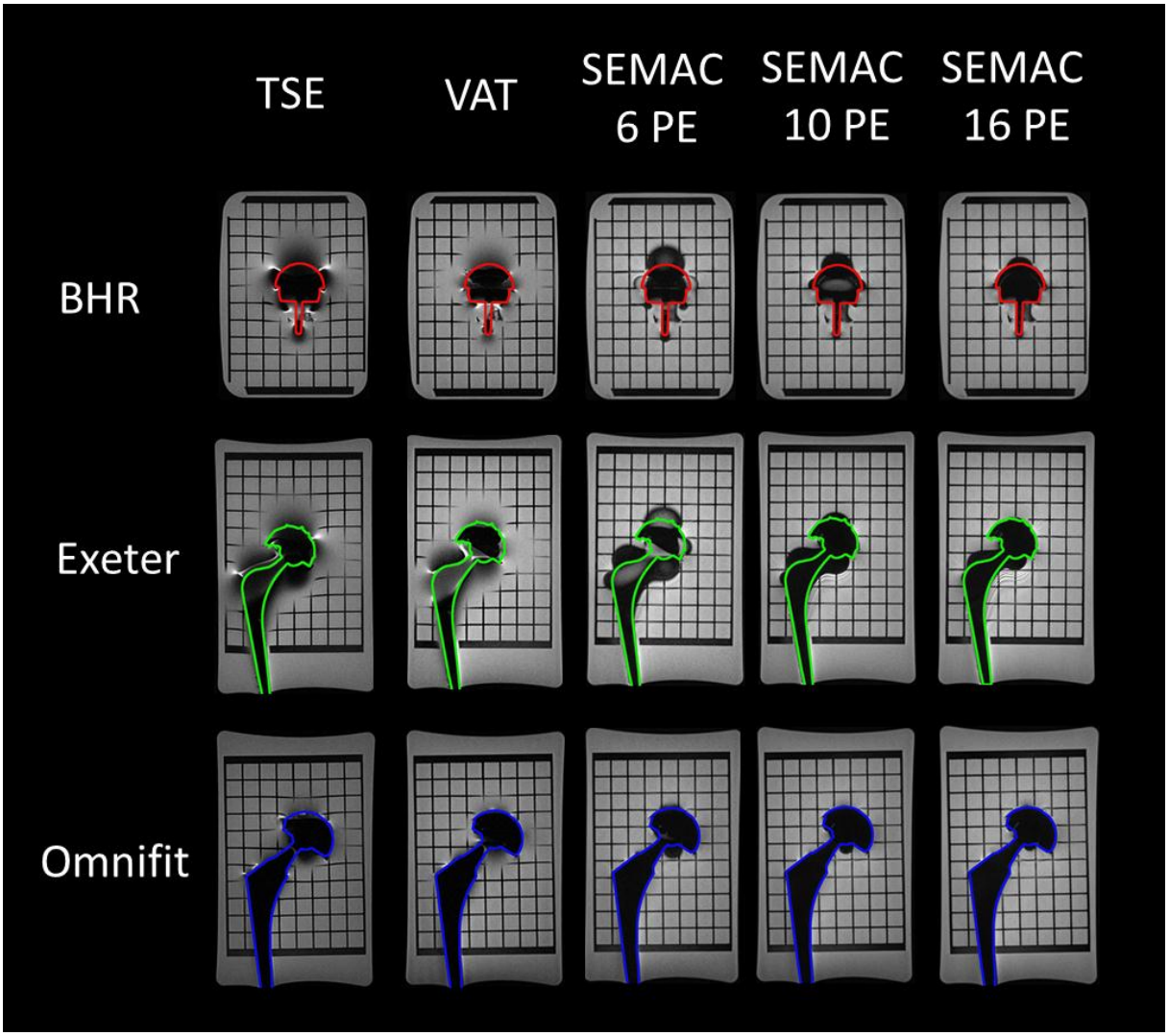

Figure 4.1 shows the MR-images on which this work is based. The TSE is the optimized protocol currently used at SUS Malmö (spring 2011). VAT is the view angle tilting version used with the Siemens WARP-sequence. SEMAC with 6, 10 and 16 phase encoding (PE) steps is the WARP-sequence using different amounts of phase encoding steps. The outlines in red, blue and green for BHR, Omnifit and Exeter respectively are the true extents of the prostheses.

4.2 Through-plane distortion quantification

The result of the through-plane distortion quantification shows an increase in visible grid length when using SEMAC and even more visible grid length when using more PE-steps. VAT does not show any improvement with this quantification method. Also worth noticing is that the Omnifit phantom shows less through-plane distortion. The results from this measurement can be seen in figure 4.2.1 below.

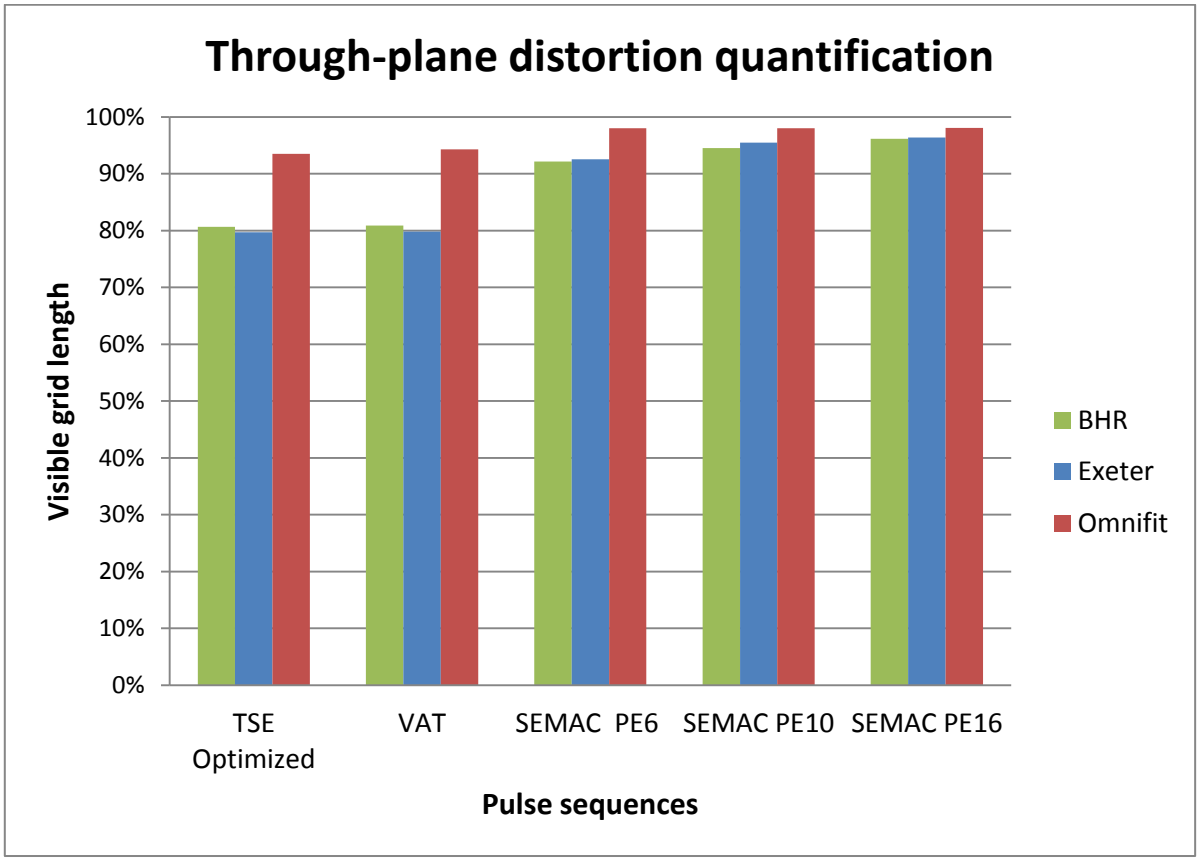

Figure 4.2.1 shows the results from the through-plane distortion quantification, with the visible grid length on the y-axis versus the pulse sequences on the x-axis. A score of 100% represents a distortion-free image.

4.3 Area measurements

The results from the area measurements can be seen in figure 4.3.1 below. It can be seen that when using the artifact measurement, the improvement made with the VAT sequence. The SEMAC sequences with more PE steps show even further improvement, except for the Exeter phantom at 6 PE steps.

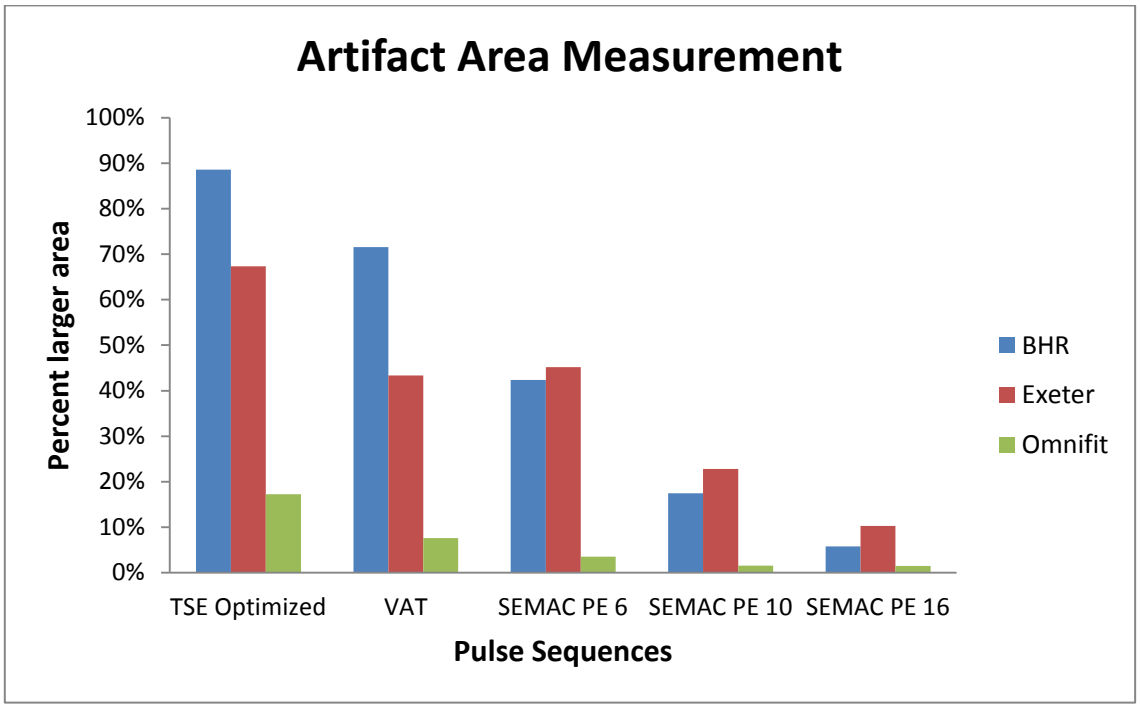

Figure 4.3.1 shows the result of the artifact area measurement with the percent larger area for the images shown on the y-axis versus the different pulse sequences on the x-axis for all the different phantoms.

4.4 Mask measurements

The results for the mask measurements are divided into the resulting artifact images received and also the calculated quantifier of total artifact ("image quality" value V).

4.4.1 Binary method

A compilation of the resulting artifact images (with absolute values) for the different pulse sequences and phantoms using the binary method (each individual image originally 512x512 pixels) can be seen in figure 4.4.1.1 below, where a perfect, artifact-free MR-image should not show any red.

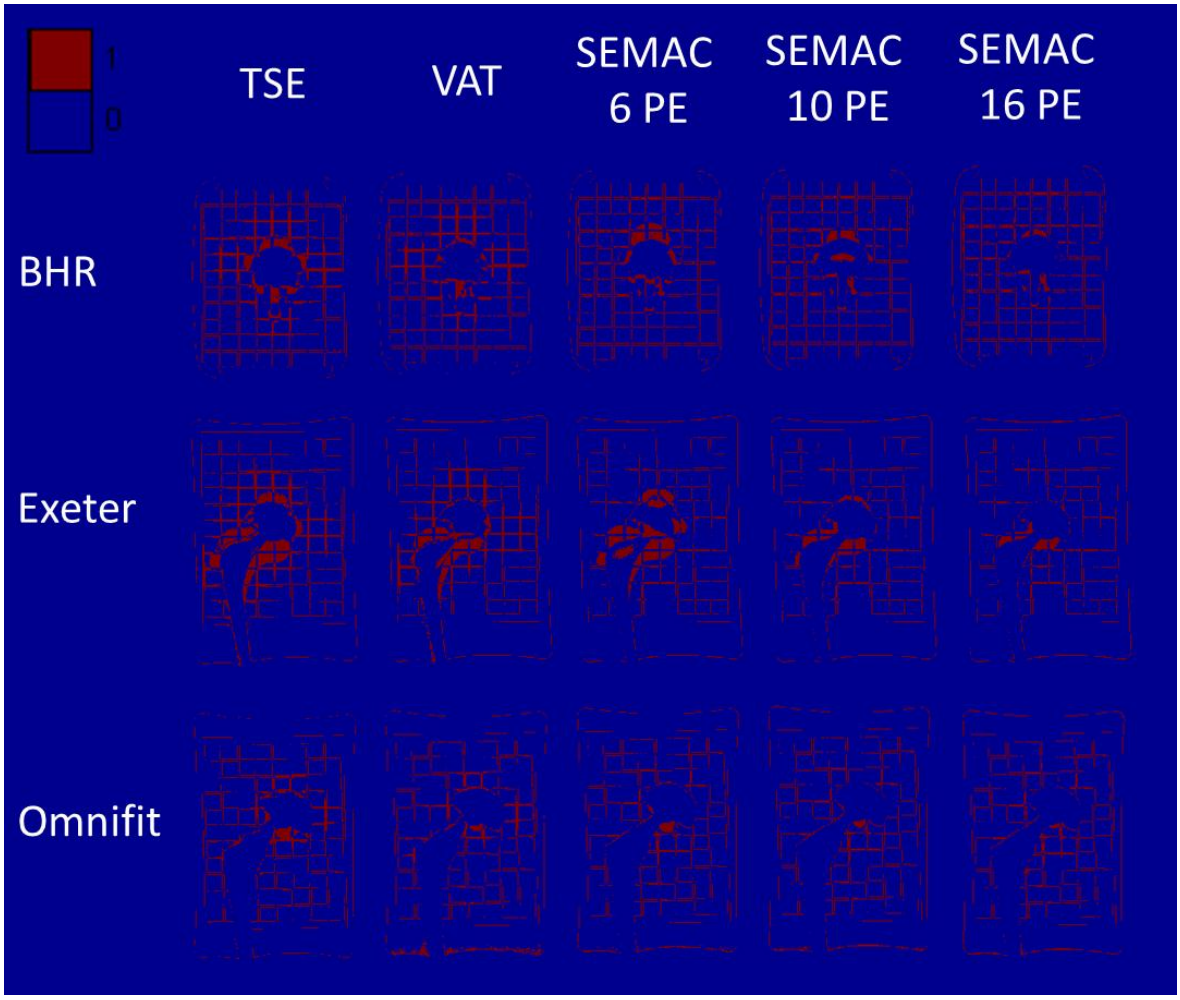

Figure 4.4.1.1 shows a compilation of the resulting artifact images acquired using the binary method mask measurement where red indicates a value of 1 and blue a value of 0, here shown on blue background.

The quantification of the different artifact images from the binary method, i.e. the sum of square of the pixel values in the images, can be seen in figure 4.4.1.2 below, where a value of zero would mean an artifact-free image. It can be seen that SEMAC with more PE steps shows less distortions. Also Omnifit shows less distortions compared to BHR and Exeter.

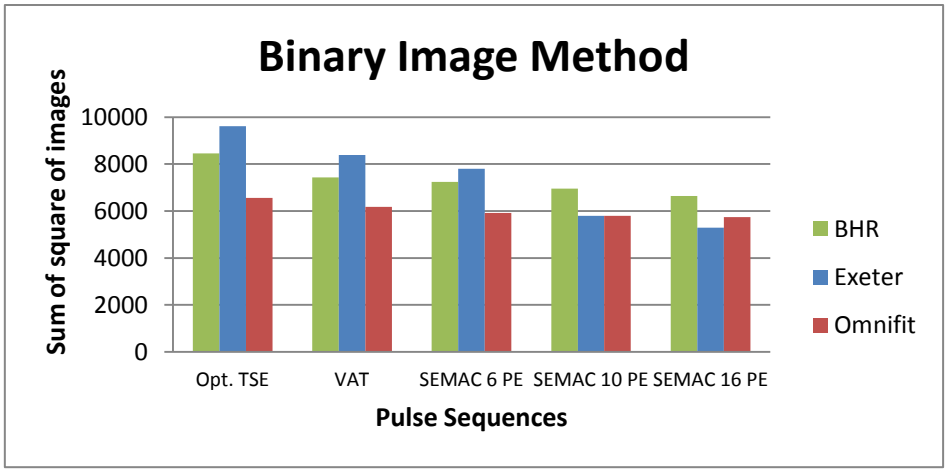

Figure 4.4.1.2 shows the resulting quantification with the result for the BHR prosthesis shown in green, the result for the Exeter prosthesis shown in blue and the Omnifit prosthesis shown in red.

4.4.2 Non-binary method: Uncorrected Gel normalization

Figure 4.4.2.1 below shows a compilation of the resulting artifact images acquired using the uncorrected gel normalization method.

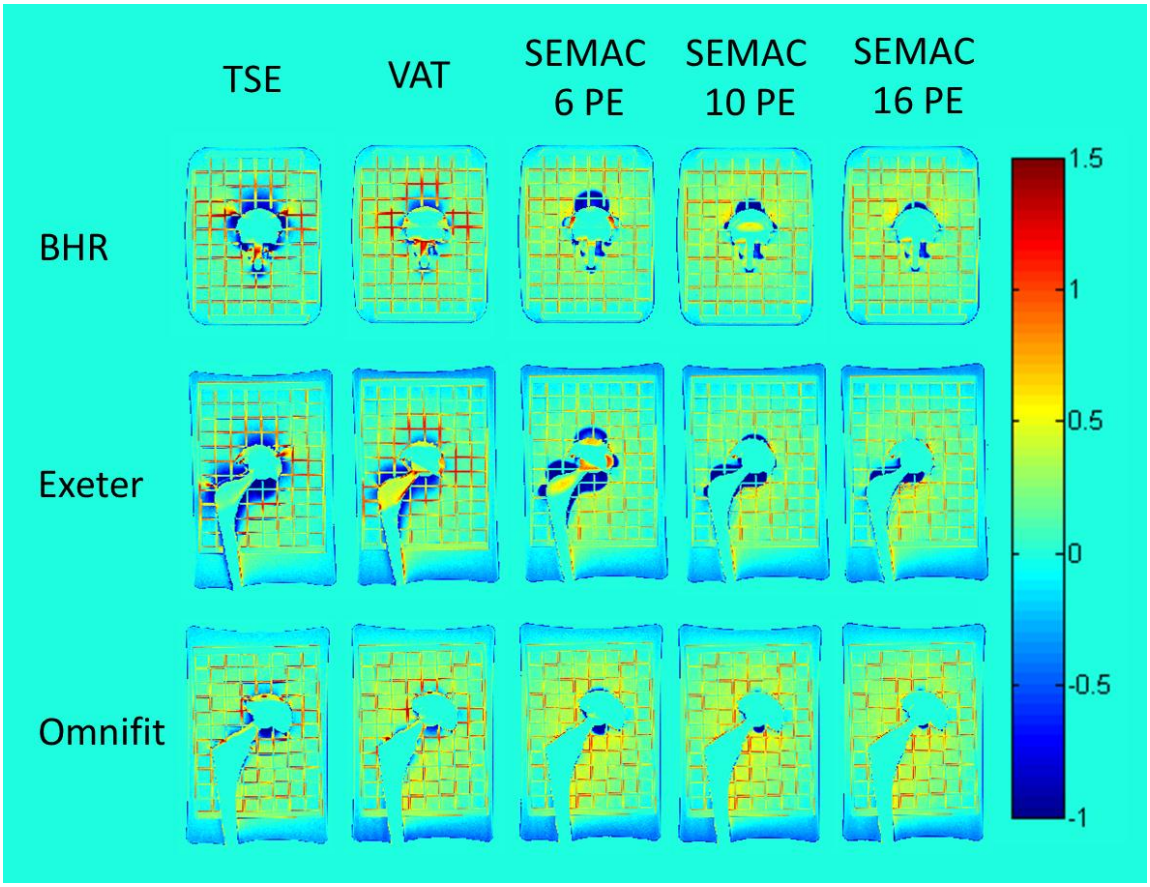

Figure 4.4.2.1 shows the resulting artifact image from the uncorrected gel normalization method. The pile up of signal can be seen as the color is moving towards red and signal loss seen as the color moving towards blue, whereas a turquoise color indicates an artifact-free pixel, which has value of zero.

The result of the quantification of the uncorrected gel normalization method for the different prostheses and pulse sequences can be seen in figure 4.4.2.2 below, where a value of 0 represents an artifact-free image.

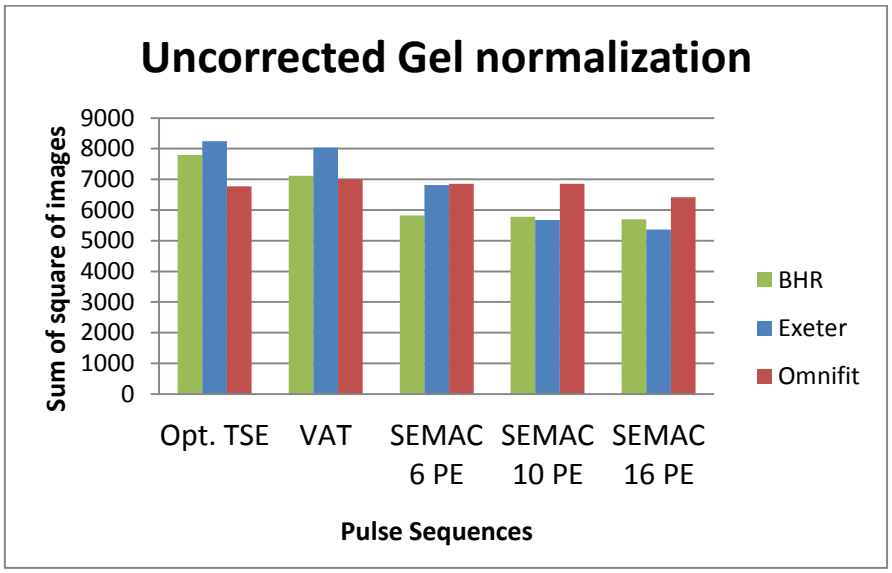

Figure 4.4.2.2 shows the resulting quantification with the result for the BHR prosthesis shown in green, the result for the Exeter prosthesis shown in blue and the Omnifit prosthesis shown in red.

4.4.3 Non-binary method: Corrected Gel normalization

A compilation of the resulting artifact images acquired from the corrected gel normalization method can be seen in figure 4.4.3.1 below. The main difference from the uncorrected method is seen as a smoother signal, not depending on the local coil insensitivities.

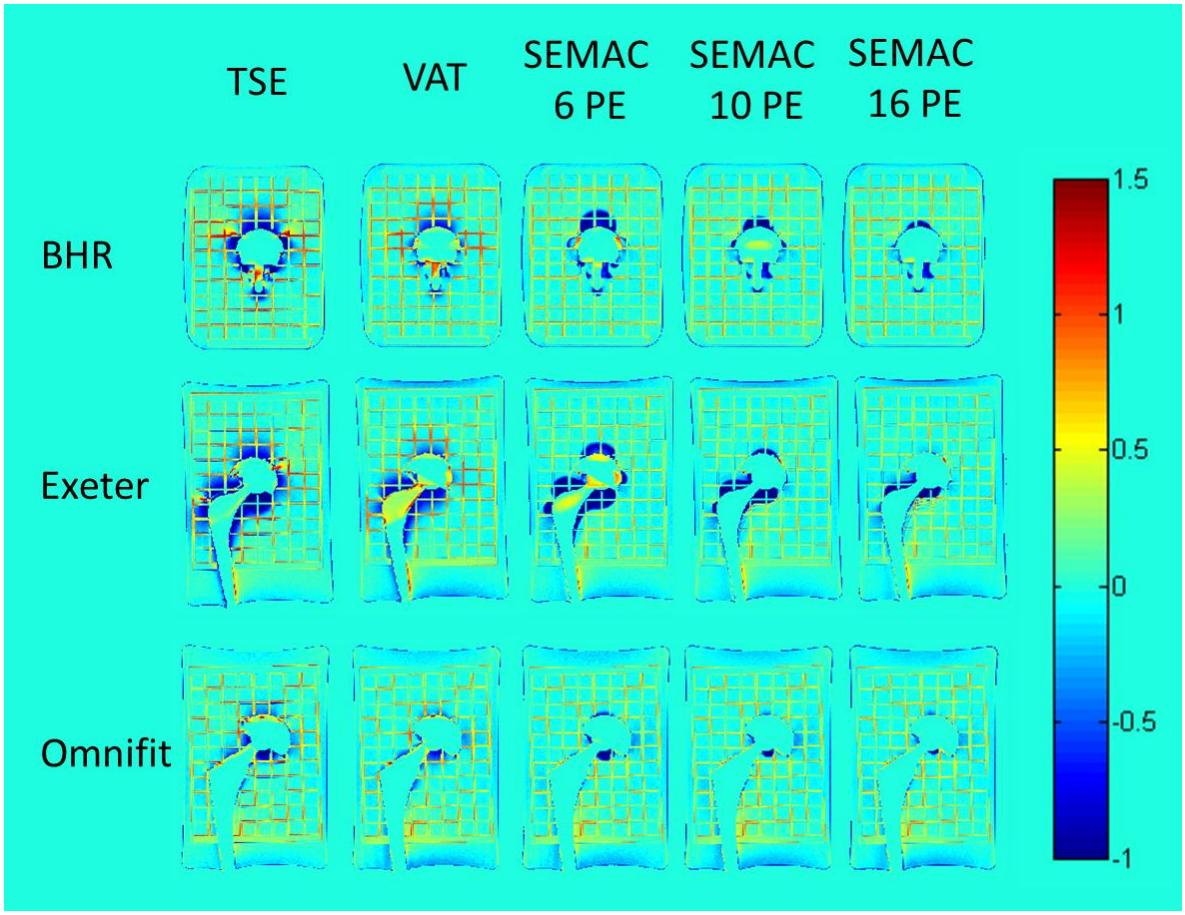

Figure 4.4.3.1 shows the resultant artifact image from the corrected gel normalization method. The pile up of signal can be seen as the color is moving towards red and signal loss seen as the color moving towards blue, whereas a turquoise color indicates an artifact-free pixel, which has value of zero

The result of the quantification of the corrected gel normalization method for the different prostheses and pulse sequences can be seen in figure 4.4.3.2 below, where a value of 0 represents an artifact-free image.

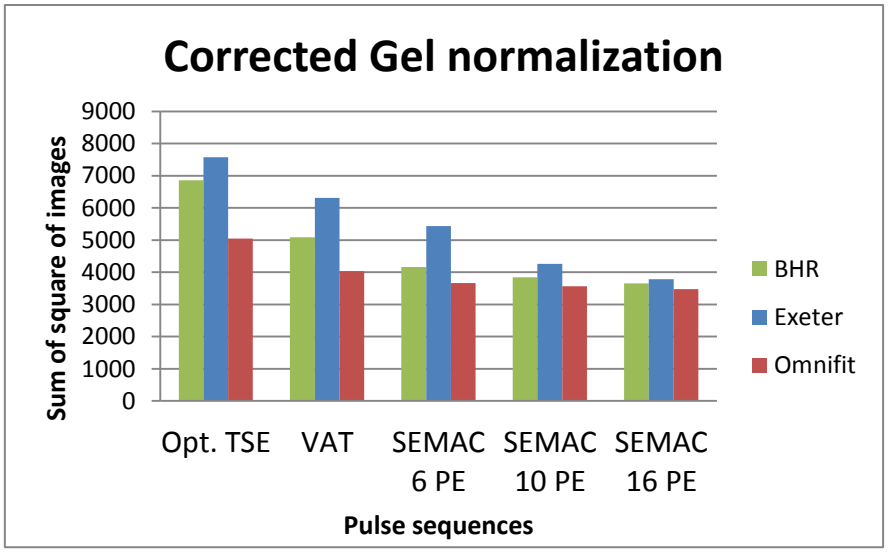

Figure 4.4.3.2 shows the resulting quantification with the result for the BHR prosthesis shown in green, the result for the Exeter prosthesis shown in blue and the Omnifit prosthesis shown in red.

5 Discussion

When observing figure 4.1, it can be seen that an improvement is made by using the VAT option and that the in-plane distortions are indeed almost completely corrected; the Perspex grid is straight and not bended when using the VAT-sequence. We also see substantially reduced distortions when the number of PE-steps is increased in the SEMAC sequence. SEMAC with 16 PE shows an almost distortion-free image for all of the phantoms, although some artifacts can be seen, especially for the Exeter phantom. This artifact, which shows signal loss near the neck of the prosthesis, has not been investigated any further in this work. The Omnifit prosthesis, which is made mainly of titanium, has low magnetic susceptibility compared to the other two prostheses and was almost perfectly reproduced using the 16 PE-steps SEMAC-sequence.

The through-plane distortion quantification show the great improvement the SEMAC sequence do to the images, mostly because the SEMAC sequence corrects the through-plane distortions which makes the reconstructed slices flat and parallel to the grid, thus making the grid more visible. As can be seen with this measurement, VAT does not show any improvement, since VAT only corrects in-plane artifacts and thus does not make the grid more visible. This measurement also shows that the Omnifit phantom shows more percentage visible grid, due to the Omnifit prosthesis being made mainly of titanium, which has the lowest magnetic susceptibility of the different prostheses in the phantoms. By using more PE steps, additional improvement can be seen for the BHR and Exeter phantoms, since more PE steps increase the range (FOV) of the through-plane distortion correction. An insufficient number of PE steps results in an aliasing of the artifacts in the z-direction. The through-plane distortions are then not completely resolved in the image, thus making it look more obscure. One concern regarding the through-plane distortion quantification measurement is that, since the visible grid length is measured by using an image-measuring tool e.g. PACS, the position

at which the visible grid length are set depends entirely on the individual who does the measurement. Therefore this measurement is highly subjective.

The artifact area measurement clearly shows the effect of implementing the new methods, where it is seen that VAT does, indeed, reduce the artifacts. It also shows that when using SEMAC the artifacts become less visible, and even less using more PE steps. Using only 6 PE steps with the SEMAC sequence, we see that the through-plane distortion correction falls short due to artifact aliasing, and for the Exeter phantom this sequence results in worse image quality and larger artifacts than the VAT-sequence, as can be seen in figure 4.1 and 4.3.1. The results also highlight the difference in artifact extent between the different materials of the prostheses. The Omnifit, for example, shows a lot less artifact area, which is to be expected due to its lower magnetic susceptibility than the other two prostheses. One problem, however, with this measurement is, that since it depends on a manually outlined artifact area, it is highly subjective; even more than the through-plane distortion quantification measurement above. This measurement can be seen as a rough way to estimate the area and to have a quick peek at the differences between phantoms.

The mask measurements were a result of an idea of comparison inspired by an article written by Kolind *et. al* [25], in which comparisons of a vax replica, which represent a "perfect" image case, and different metal reducing techniques, which shows distortions etc., are made. For the measurements in the present study, a vax replica was not present, so the idea was instead to use the best SEMAC sequence and the x-ray projections of the prostheses to try to create a binary image, representing a "perfect" distortion-free image, and then to compare the different methods with this "perfect" image. This was, however, not complication-free since after creating these "perfect" images, they needed to be able to comparable to the resulting MR-images. This resulted in the three different measurements made.

Another approach of evaluation is to generate images both with and without the implant present, i.e. using a reference image (without the implant) and an implant image (with the implant), both using the exact same parameters and then compute the differences outside the region corresponding to the implant between reference and implant images. This method, described in ASTM F2119-01 [26] has been adopted and used by Olsrud *et. al* [27] in combination with a fixed threshold and an automatic pixel count for area measurement. This method could be used in further studies and be compared to the artifact area measurement used in this work to give a more thorough understanding, however this would require a new phantom to be made in order to achieve the reference image without the implant.

The first measurement, called the binary image method, was the result of making the MR-images binary in order to be directly comparable with the binary "perfect" images. However these results did not fully take in mind the signal pile-ups and loss of signal which we also would like to compare. The result of this measurement show that VAT indeed is a better method than the optimized TSE, and that SEMAC with more PE also achieves a more artifact-free image. Also note that the result of the binary image method is highly dependent on the threshold chosen to create the binary MR-images. In this work, that threshold was chosen to be roughly in the middle between the highest (gel) and lowest (grid) occurring

signal in an area where the signal is unaffected by metal artifacts, this was thought to be the best threshold value, although there could be an investigation of which threshold is the best one, such investigation was not made, due to the fact that the binary image method was not a very reliable method and that the signal pile-ups and loss also needed to be included in the measurement.

The flaws of the binary image method resulted in the uncorrected gel normalization method, which better should take the signal pile-ups and signal loss in consideration. The result of this method is very confusing, were e.g. the optimized TSE is ranked unexpectedly well for the Omnifit prosthesis (Figure 4.4.2.2). This might be due to the problem of not having a coil-sensitivity correction which was made in the last method.

The last method in this master thesis, the corrected gel normalization method, is similar to the uncorrected gel normalization method, but additionally corrects for intensity variations in the image due to spatially variant RF-coil sensitivities. This method also manages to quantitatively represent the visual impression of the MR-images; that there is an improvement by using the VAT-sequence and that SEMAC with more PE steps achieve greatly improved image quality and artifact suppression. If one would consider comparing the different prostheses with regard to their magnetic susceptibility, one would intuitively expect the prostheses with highest susceptibility to produce the most severe artifacts. The results are consistent with this expectation, because Exeter, made of stainless steel, shows a higher distortion score (V) than BHR (made of Co-Cr) while Omnifit (made of titanium) shows the least distortion score. However an exact comparison cannot be made based on this work, one has to consider the size and other factors if one would try to compare the magnetic susceptibility.

The biggest problems with the mask methods are the need of a MR-image (the best SEMAC sequence in this case) to create the mask itself, resulting in uncertainty and a risk of the mask itself being distorted. Another issue is the resolution of the mask image; only 512x512 pixels might be too low. Also the correction of the local coil insensitivities is not perfect. There is several solutions to these problems, one including using a grid with high density, making it appear visible when using x-ray scans. With x-ray images a mask would be able to be generated without using MR-images. Such an image would also have a higher resolution. Another way of solving the problem with the low-resolution mask is to use a non-binary mask, which would also solve the problem with the irregular image intensity, having roughly the same intensity variation on the image and the mask.

It can be said that the methods developed in this work can be improved upon further. It should be noted that the “perfect” mask against which all the images are compared is not truly perfect, since it is binary. No MR-image is binary in itself, so it would be better to try to recreate a “perfect” image which has the signal variations and that would in itself be a better way to compare the images. This non-perfect mask explains that the artifact-images show artifacts far away from the prostheses, where one would not expect any signal variation at all. This is apparent in figures 4.4.1.1, 4.4.2.1 and 4.4.3.1, where nearly all interfaces to the grid are scored as artifacts. Another way to try to reduce this is by increasing the resolution of the

mask, so that the transition between signal and no-signal is not that rough, in this work the mask was 512x512 pixels, it could be increased to even more and then in turn compare it to MR-images of the different sequences using a higher resolution. Also worth mentioning is that the binary image method results highly depends on the threshold chosen for the creation of the binary MR images.

The current method of evaluation in this work is limited to the artifacts in a single plane; however it is a volume that is affected around the prosthesis. If one would instead try to evaluate such a volume a substantially more complicated phantom design and evaluation, compared to the ones used in this work, would be required. This was not possible to implement within the scope of the present work.

6 Conclusion

Through-plane distortions were successfully quantified by measuring the length of the visible gridlines. In-plane distortions, quantified by measuring the artifact areas with regions of interest, were also able to produce a result in agreement with the visual impressions of the artifacts, however with the drawback of requiring operator dependent and subjective ROI-drawing. The mask based methods have potential for quantifying both in-plane and through-plane distortions simultaneously without user input. These methods, however, still require further improvements to achieve that goal. The VAT-sequence reduced much of the in-plane distortions, but no through-plane distortions. The SEMAC-sequence reduced both in-plane and through-plane distortions, however in this study, at least 16 z-phase encoding steps were needed, which requires a very long scan time. The results demonstrate that the effects of pulse sequence type, parameter settings, and prosthesis material can be quantitatively evaluated by the proposed grid-based phantom and analysis methods.

7 References

1. Kurtz, S., et al., *Prevalence of primary and revision total hip and knee arthroplasty in the United States from 1990 to 2002.* Journal of Bone and Joint Surgery - American Volume, 2005. **87**: p. 1487-1497.
2. Kurtz, S., et al., *Projections of primary and revision hip and knee arthroplasty in the United States from 2005 to 2030.* Journal of Bone and Joint Surgery - American Volume, 2007. **89-A**: p. 780-785.
3. Mahendra, G., et al., *Necrotic and inflammatory changes in metal-on-metal resurfacing hip arthroplasties.* Acta Orthop, 2009. **80**(6): p. 653-9.
4. Carrothers, A.D., et al., *Birmingham hip resurfacing: the prevalence of failure.* J Bone Joint Surg Br, 2010. **92**(10): p. 1344-50.
5. Potter, H.G., et al., *Magnetic resonance imaging after total hip arthroplasty: evaluation of perioprosthetic soft tissue.* Journal of Bone and Joint Surgery - American Volume, 2004. **86-A**: p. 1947-1954.
6. Puri, L., et al., *Use of helical computed tomography for the assessment of acetabular osteolysis after total hip arthroplasty.* Journal of Bone and Joint Surgery - American Volume, 2002. **84**: p. 609-614.
7. Olsen, R.V., et al., *Metal artifact reduction sequence: Early clinical applications.* Radiographics, 2000. **20**: p. 699-712.
8. Ludeke, K.M., P. Roschmann, and R. Tischler, *Susceptibility artefacts in NMR imaging.* Magnetic Resonance Imaging, 1985. **3**: p. 329-343.
9. Balcom, B.J., et al., *Single-Point Ramped Imaging with T1 Enhancement (SPRITE).* Journal of Magnetic Resonance, 1996. **123**: p. 53-61.
10. Venook, R., et al., *Prepolarized magnetic resonance imaging around metal orthopedic implants.* Magnetic Resonance in Medicine, 2006. **56**: p. 177-186.
11. Moessle, M., et al., *SQUID-detected microtesla MRI in the presence of metal.* Journal of Magnetic Resonance, 2006. **179**: p. 146-151.
12. Chang, H. and J. Fitzpatrick, *A Technique for Accurate Magnetic Resonance Imaging in the Presence of Field Inhomogeneities.* IEEE Transactions on Medical Imaging, 1992. **11**: p. 319-329.
13. Skare, S. and J.L.R. Andersson, *Correction of MR Image Distortions Induced by Metallic Objects Using a 3D Cubic B-Spline Basis Set: Application to*

Stereotactic Surgical Planning. Magnetic Resonance in Medicine, 2005. **54**: p. 169-181.
14. Robson, M., et al., *Magnetic Resonance: An Introduction to Ultrashort TE (UTE) Imaging.* Journal of Computer Assisted Tomography, 2003. **276**: p. 825-846.
15. Idiyatullin, D., et al., *Fast and Quiet MRI Using a Swept Radiofrequency.* Journal of Magnetic Resonance, 2006. **1812**: p. 342-349.
16. Cho, Z.H., D.J. Kim, and Y.K. Kim, *Total inhomogeneity correction including chemical shifts and susceptibility by view angle tilting.* Magnetic Resonance in Medicine, 1987. **15**: p. 7-11.
17. Lu, W., et al., *SEMAC: Slice Encoding for Metal Artifact Correction in MRI.* Magnetic Resonance in Medicine, 2009. **62**: p. 66-76.
18. K.M. Koch, P., et al., *A Multispectral Three-Dimensional Acquisition Technique for Imaging Near Metal Implants.* Magnetic Resonance in Medicine, 2009. **61**: p. 381-390.
19. Lee, M.J., et al., *Quantitative assessment of an MR technique for reducing metal artifact: application to spin-echo imaging in a phantom.* Skeletal Radiology, 2001. **30**: p. 398-401.
20. K. Butts, P., et al., *Management of Biopsy Needle Artifacts: Techniques for RF-Refocused MRI.* Journal of Magnetic Resonance Imaging, 1999. **9**: p. 586-595.
21. K. Butts, P., J.M. Pauly, and G.E. Gold, *Reduction of Blurring in View Angle Tilting MRI.* Magnetic Resonance in Medicine, 2005. **53**: p. 418-424.
22. Brian A. Hargreaves, P., et al., *Accelerated Slice Encoding for Metal Artifact Correction.* Journal of Magnetic Resonance Imaging, 2010. **31**: p. 987-996.
23. Nishimura, D., *Principles of Magnetic Resonance Imaging.* Stanford: Stanford University, 1996.
24. Speier, P. and F. Trautwein, *A Calibration for Radial Imaging with Large Inplane Shifts.* In: Proceedings of the 13th Annual Meeting of ISMRM, Miami, 2005: p. 2295.
25. S.H. Kolind, M., et al., *Quantitive Evaluation of Metal Artifact Reduction.* Journal of Magnetic Resonance Imaging, 2004. **20**: p. 487-495.
26. *American Society for Testing and Materials (ASTM) F2119-01: Standard Test Method for Evaluation of MR Image Artifacts from Passive Implants.* ASTM International, West Conshohocken, PA, 2001.
27. Olsrud, J., et al., *Magnetic Resonance Imaging Artifacts Caused by Aneurysm Clips and Shunt Valves: Dependence on Field Strength (1.5 and 3 T) and Imaging Parameters.* Journal of Magnetic Resonance Imaging, 2005. **22**: p. 433-437.